Proceedings of the Seventh International Conference on
Railway Technology: Research, Development and Maintenance
Edited by: J. Pombo
Civil-Comp Conferences, Volume 15, Paper 19.7
Civil-Comp Press, Edinburgh, United Kingdom, 2026
ISSN: 2753-3239, doi: 10.4203/ccc.15.19.7

Study on a Hybrid Finite Element-Ray Method for Predicting Broadband Interior Structure-Borne Noise

X. Liang[1], B. Hou[1], J. Pombo[2], Y. Zhang[1], W. Zhou[1], Q. Zhang[1] and H. Ban[1]

[1]School of Civil Engineering, Beijing Jiaotong University, China
[2]Institute of Railway Research, University of Huddersfield, United Kingdom

Abstract

Interior structure-borne noise directly affects human comfort. Its accurate prediction is key in noise-control engineering. Traditional single numerical methods struggle to balance accuracy and efficiency across the entire frequency range. To address this problem, a broadband prediction method is proposed in this paper, which fuses the low-frequency finite element method with the high-frequency ray acoustics method. A two-dimensional simulation example is constructed for verification. The results show that the ray acoustics method exhibits low sensitivity to mesh size. Its computational characteristics are primarily determined by the number of released rays. In the 400 to 1000 Hz frequency band, the spectral trends of the sound pressure level calculated by the ray acoustics method and the finite element method are generally similar. The mean absolute error of their one-third-octave-band sound pressure level is only 1.14 dB. Under equivalent computational efficiency, the prediction error of the ray acoustics is 1.58 dB lower than that of the finite element method with a coarse mesh, demonstrating superior performance in the high-frequency band.

Keywords: hybrid acoustic modeling, structure-borne noise, railway induced noise and vibration, ray acoustics, high-frequency noise, finite element modeling (FEM).

1 Introduction

With the continuing expansion of China's urban rail transit networks under the strategic background of building a strong transportation nation, building interior structure-borne noise induced by train operation has become increasingly prominent. It affects acoustic comfort for residents along railway corridors and may interfere with the normal operation of precision instruments. This has become a core difficulty in environmental noise control for urban rail transit. Accurate broadband prediction of this noise is a crucial prerequisite for vibration mitigation and noise-control design.

Considerable research has been conducted by domestic and international scholars on the prediction of train-induced interior structure-borne noise in buildings. These studies are mainly divided into empirical formulae and numerical methods. Empirical formulae are widely used because they are convenient and efficient. Kurzweil [1] established an early prediction formula for interior structure-borne noise based on field measurements of buildings along underground railway lines. Melke [2] proposed a structure-borne noise prediction procedure based on the assumptions of floor-radiation dominance and equivalent radiation from all room surfaces. Subsequently, corresponding industrial empirical prediction standards were issued in countries such as the United States [3] and Austria [4]. Recently, Zou et al. [5] attempted to combine field measurement with deep learning to predict interior structure-borne noise. Although such methods have high computational efficiency, they are often constrained by site-specific measurement conditions or idealised model assumptions. Their adaptability to complex non-standard buildings and unbuilt projects remains relatively limited.

With the development of computer technology, numerical simulation has become an important approach for predicting train-induced building vibration and interior structure-borne noise. Sadeghi and et al. [6] used the finite element method (FEM) to analyse vibration propagation and structure-borne noise in building foundations. Nagy and et al. [7] proposed an improved interior structure-borne noise prediction method based on global Rayleigh reflectance and the direct boundary element method (BEM). However, the meshing difficulty of the FEM and BEM increases sharply with frequency, leading to a significant decrease in computational efficiency. For mid- and high-frequency vibro-acoustic problems, statistical energy analysis (SEA) has been widely used with high computational efficiency and accuracy [8, 9]. However, because it is based on the energy statistical average assumption, it is difficult to accurately describe the local sound pressure distribution and specific propagation paths in interior spaces. By contrast, the ray acoustics method exhibits significant advantages in the geometrical acoustics range [10]. By tracing the reflection, absorption and energy evolution trajectories of sound rays at boundaries, it can efficiently and accurately simulate the local sound field environment in complex spaces.

On this basis, this paper proposes a broadband hybrid acoustic prediction method combining the FEM at low frequencies with the ray acoustic at high frequencies. The advantageous frequency ranges and the transition boundary of the two approaches are identified. This achieves accurate and efficient broadband prediction of this noise, providing technical support for the vibration mitigation and noise-control design of buildings along rail transit lines.

2 Methods

2.1 Hybrid modelling framework

Indoor acoustics can be divided into three categories based on the frequency range. In the low-frequency range, the acoustic response of a room is dominated by discrete room resonant modes. This range is a typical mode-controlled region. As the frequency increases, the acoustic wavelength decreases and becomes much smaller than the geometric dimensions of the room. Consequently, the modal density increases sharply, and the sound field distribution tends to be statistically uniform, which marks the transition into the geometrical acoustics region. A transition region exists between the mode-controlled and geometrical acoustics regions. The Schroeder frequency (fc) is typically used as the critical boundary point, which is given by Equation (1).

$$f_c = 2000 \lg \frac{\sqrt{T_{60}}}{\sqrt{V}} \tag{1}$$

In the equation: T_{60} is the reverberation time in seconds and V is the room volume in cubic metres.

This study proposes a broadband interior acoustic modelling method. In Figure 1 the specific technical route is shown. The FEM is used at low frequencies. By solving the wave equation, it accurately simulates the standing wave characteristics and modal coupling of the low-frequency sound field. The ray acoustics method is used at high frequencies. It simulates the high-frequency sound field by tracing the propagation and reflection trajectories of sound ray particles carrying acoustic energy. This avoids the strict limitation on mesh density in large-degree-of-freedom calculations of the FEM and significantly improves the computational efficiency of the high-frequency sound field solution.

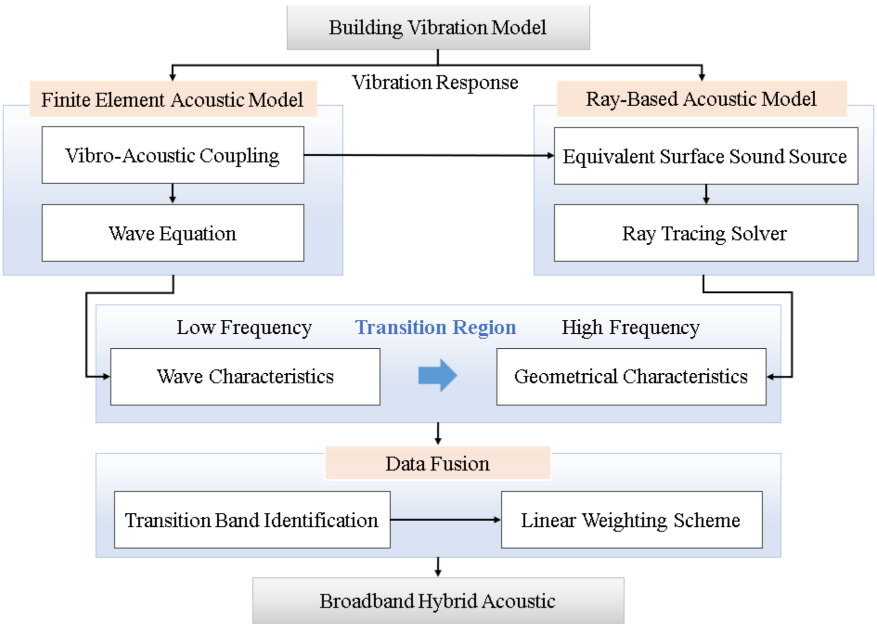

Figure 1: Technical route.

The transition frequency band is determined by comparing the spectral trends and error analyses of the two methods. Methods such as the linear gradient weighting method are then used to achieve a smooth transition and fusion of the predicted results. This process ensures the continuous variation of the sound pressure level curve. Consequently, an interior structure-borne noise prediction method that balances both accuracy and efficiency is constructed.

2.2 Two-dimensional model construction

To verify the feasibility of the broadband hybrid prediction method, a two-dimensional (2D) model is selected as the research object. A finite element acoustic model and a ray acoustics model are constructed separately to simulate the secondary noise induced by wall vibration.

2.2.1 Finite element acoustic model

In Figure 2 the components of the finite element acoustic model are shown. The periphery of the model is the wall structure. It is rigidly fixed at its four corners. The interior is the acoustic air domain. The material properties of the model are given in Table 1.

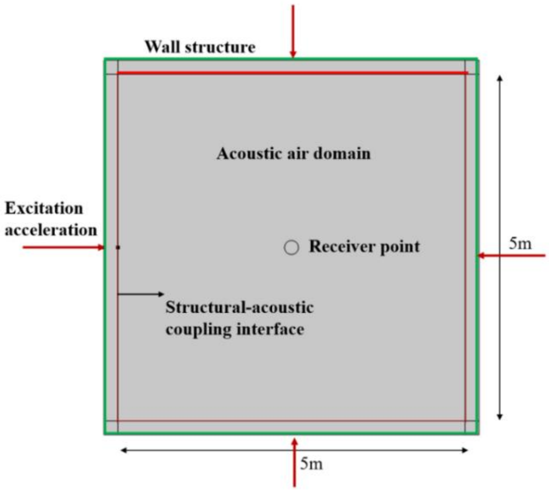

Figure 2: Finite element acoustic model schematic

Component	Parameter	Value	Unit
Building structure	Elastic modulus	2.5×10^{10}	Pa
	Density	2400	kg/ m^3
	Poisson's ratio	0.2	-
	Damping ratio	0.05	-
Air domain	Attenuation coefficient	0.3	dB/m
	Speed of sound	343	m/s
	Density (air)	1	kg/ m^3

Table 1: Material parameters of the finite element acoustic model

A frequency-response analysis method is used in this study to solve the model. By applying a specified acceleration excitation to the wall boundaries, the vibration response of the wall structure is obtained. Meanwhile, the interface between the wall and the air domain is defined as a vibro-acoustic coupling interface. The vibration velocity field of the wall structure is mapped as the acoustic boundary condition of the fluid domain. Consequently, the solution and analysis of the interior acoustic environment are completed.

2.2.2 Ray acoustic model

In Figure 3 the components of the ray acoustic model are shown. A finite element interlayer is used to calculate the vibration-induced surface near-field acoustic radiation. At the interface between the finite element and ray acoustic domains, the boundary normal sound intensity of the finite element domain is integrated along the envelope segment. This calculates the total source sound power per unit thickness. Based on this power, a specified number of sound ray particles carrying energy are released to simulate sound propagation.

The energy evolution of the sound ray particles in the space follows the principles of medium absorption attenuation and wall reflection loss. When the sound rays pass through the target receiving domain, the acoustic response characteristics are reconstructed using the ray power and propagation time information carried by the sound rays.

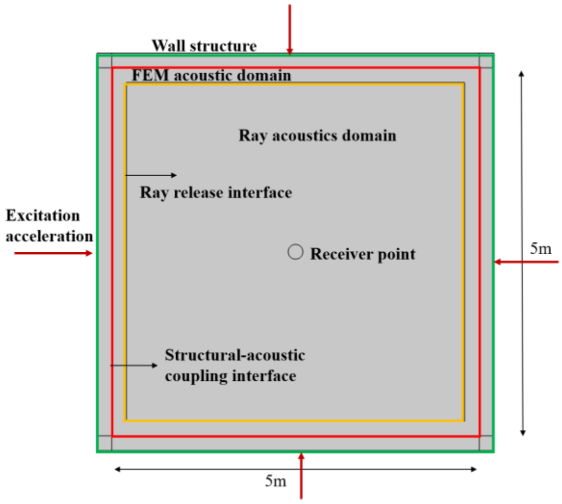

Figure 3: Ray acoustic model schematic

2.3 Computational parameter selection

The numerical calculations were performed on a dual-socket Intel64 processor system equipped with two high-performance Intel(R) processors (Family 6, Model 85) and 48 cores in total.

2.3.1 Finite element acoustic model mesh size

For the finite element acoustic model, a free triangular mesh was adopted. According to the acoustic wavelength relation $\lambda = c/f_{max}$, the 800-1000 Hz frequency band was selected for frequency-domain analysis. The minimum wavelength was $\lambda_{min}=c/f_{max}=0.343m$. The maximum mesh element sizes were set as λ/5, λ/6, λ/8, λ/10, λ/15 and λ/20.

The computation of the sound pressure level error at receiver 1 for each mesh is given by Equation (2). The calculation result corresponding to a maximum mesh size of λ/20 is taken as the accuracy reference. In Figure 4 the resulting calculation errors are shown

$$Error_{dB}|_f = 20\log 10 \frac{\left\| E(f) - E_{ref}(f) \right\|}{\left\| E_{ref_{\max}}(f) \right\|} \tag{2}$$

In the equation: $Error_{dB|f}$ is the spectrum error at frequency f, $E(f)$ is the calculated spectrum value, $E_{ref}(f)$ is the reference spectrum value, and $E_{refmax}(f)$ is the maximum amplitude of the reference spectrum within the frequency band.

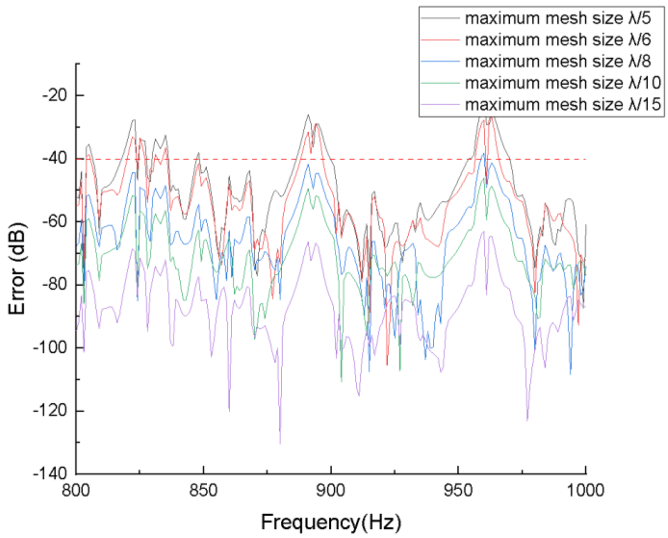

Figure 4: Sound pressure level errors for different maximum mesh sizes.

The curves show that the calculated error at the receiver decreases monotonically as the maximum mesh size is reduced. In this study, an error below -40 dB is taken as the criterion for mesh-independence satisfaction. When the maximum mesh size is smaller than λ/8, the receiver error remains below -40 dB. This satisfies the mesh-independence requirement. Therefore, the maximum mesh size in the finite element simulation is selected to be smaller than λ/8.

2.3.2 Ray acoustic model mesh size

For the ray acoustic model, the total number of rays was fixed at 5000, and five maximum mesh sizes of 0.1 m, 0.3 m, 0.5 m, 0.7 m and 0.9 m were compared. The computation of the sound pressure level error is given by Equation (2), where the calculation result obtained with the maximum mesh size of 0.1 m is taken as the accuracy reference. In Figure 5 the resulting calculation errors are shown and in Table 2 the computation times are listed. When the mesh size increases from 0.1 m to 0.3

m, the computation time is reduced by 7 s. Further mesh coarsening has little influence on either computational efficiency or accuracy, and the errors in the frequency band remain below - 40 dB. This occurs because, in ray-tracing simulation, the mesh is used only for spatial sampling. Provided that the resolution requirement is met, changes in mesh scale do not significantly affect the computational cost. Therefore, the maximum mesh size in the ray acoustic simulation is set to 0.3 m.

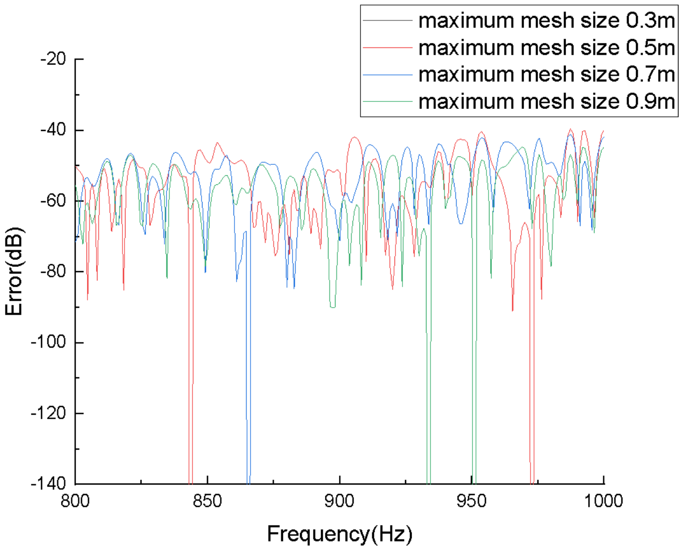

Figure 5: Sound pressure level errors for different maximum mesh sizes.

Maximum mesh size [m]	Computation time [s]
0.1	63
0.3	55
0.5	55
0.7	54
0.9	54

Table 2: Computation times for different maximum mesh sizes.

2.3.3 Number of rays

The number of rays directly affects the ray sampling at the receiver. If too few rays are emitted, the receiver is insufficiently sampled. This increases the sound pressure prediction error. In this calculation, the maximum mesh size is fixed at 0.3 m. The computation of the sound pressure level error is given by Equation (2). The calculation result obtained with 5000 rays is taken as the accuracy reference to compare the prediction accuracy under the conditions of 1000 to 4000 rays. In Figure 6 the computation times are listed and in Table 6 the sound pressure level error curves are shown. The computation time increases with the number of rays. When 4000 rays are used, the overall error remains below -20 dB. This indicates that the model has converged. Therefore, 5000 rays are adopted in the ray acoustic simulation for this study.

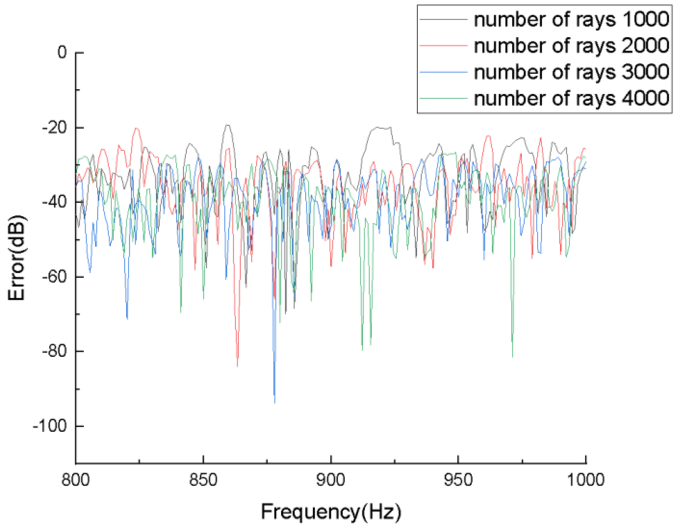

Figure 6: Sound pressure level errors for different numbers of released rays.

Number of rays	Computation time [s]
1000	44
2000	45
300	46
4000	49
5000	54

Table 3: Computation times for different numbers of released rays.

3 Result

3.1 Comparative analysis of model results

The mesh generation of the finite element model satisfies the accuracy requirements for sound field calculations. Therefore, the full-frequency sound pressure level obtained by the finite element method is taken as the reference truth value. This baseline is used to verify the accuracy of the calculation results obtained by the ray acoustics method.

In Figure 7 the significant differences between the ray acoustic and finite element predictions are shown in the low-frequency range due to modal effects. As the frequency increases, the modal superposition effect becomes stronger. Consequently, the difference between the two methods gradually decreases, and the spectral trends tend to become consistent.

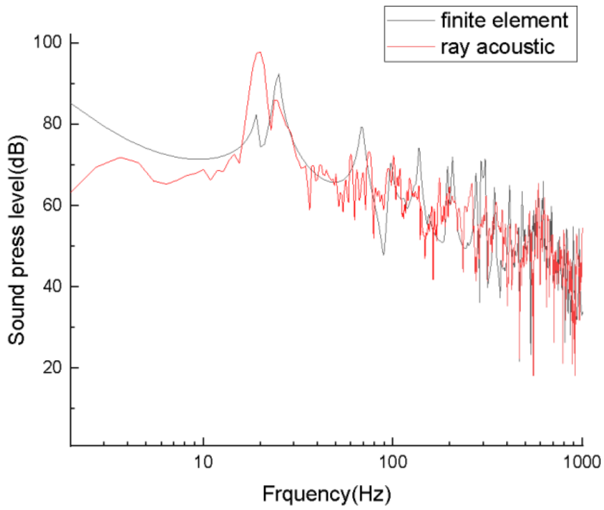

Figure 7: Comparison of sound pressure level spectra.

3.2 Data fusion

After the independent calculations of the finite element and ray acoustic sound fields are completed, a data fusion strategy is required to connect the two results over the broadband range. Accurate identification of the transition interval is critical to the fusion quality. In Figure 8 a favorable transition characteristic is shown in the 350-450 Hz range for the finite element and ray acoustic spectra. Above 400 Hz, the trends of the two methods become consistent. In Figure 9 the one-third-octave-band sound pressure level comparison and the calculation error of the ray acoustics method relative to the finite element method are shown. The results indicate that the sound pressure level variation of the two methods remains highly consistent in the 400-1000 Hz band. The error at each center frequency is below 3 dB, and the overall mean absolute error (MAE) is 1.14 dB.

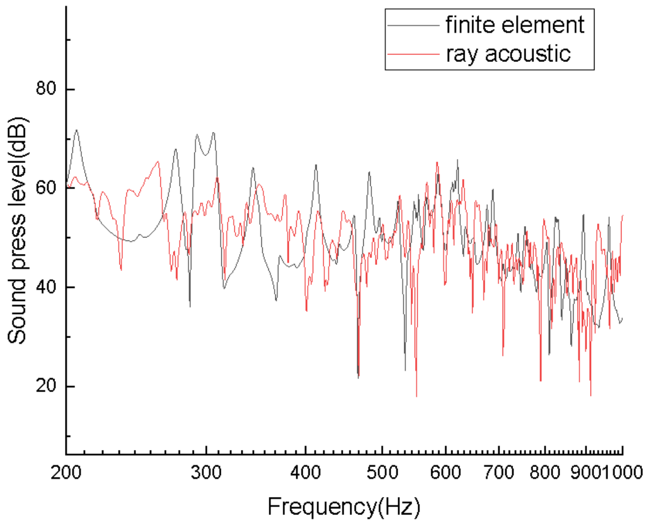

Figure 8: Local sound pressure level spectrogram.

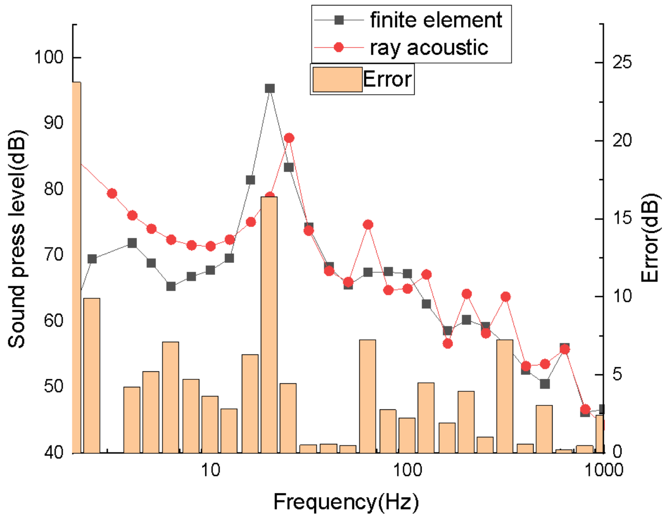

Figure 9: One-third-octave-band sound pressure level comparison and error analysis.

Based on these results, the finite element method is used in the 1-350 Hz band, and the ray acoustics method is applied above 400 Hz. In the 350-400 Hz transition region, a linear gradient weighting method is used to complete the transition and fusion. The computation of the fused sound pressure level L in the transition region is given by Equation (3). In Figure 10 the transition-region connection curve after data fusion is shown.

$$SPL_f = (1-w)\cdot SPL_{FEM} + w\cdot SPL_{Ray} \tag{3}$$

In the equation: $w=\frac{f-350}{400-350}$, SPL_{FEM} is the finite element sound pressure level, SPL_{Ray} is the ray acoustic sound pressure level, and SPL_f is the fused final sound pressure level.

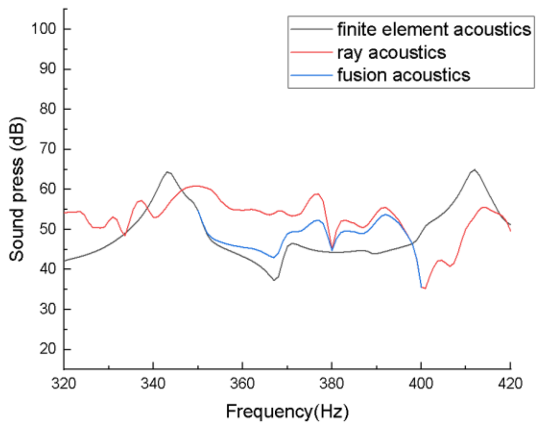

Figure 10: Connection and fusion curves in the transition region.

To verify the computational efficiency advantage of the ray acoustics method, the finite element mesh is coarsened. In the 400-1000 Hz band, the computation time of the finite element method is reduced to 113 s. This is of the same order as the 105 s required by the ray acoustics method. In Figure 11 the one-third-octave-band sound pressure level comparison is shown. The coarsened finite element model reproduces the sound pressure level trend less accurately than the ray acoustics method. The mean absolute error is 2.716 dB, which is 1.576 dB higher than that of the ray acoustics method. Overall, the ray acoustics method demonstrates better performance in this frequency band.

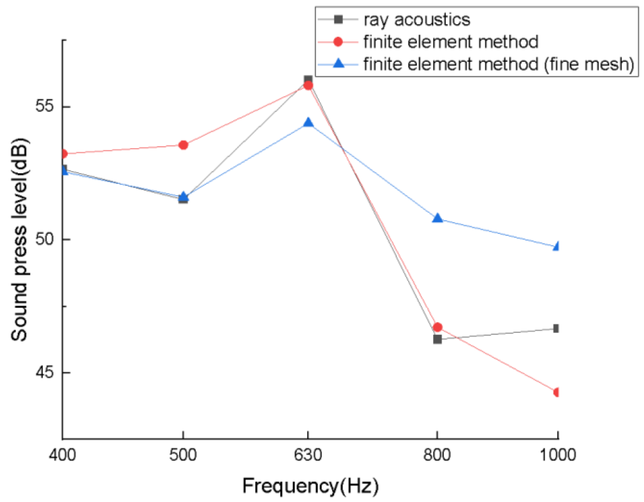

Figure 11: One-third-octave-band sound pressure level comparison.

4 Conclusions and Contributions

This paper addresses the difficulty of achieving both accuracy and efficiency with a single numerical method for broadband prediction of interior secondary noise. A hybrid acoustic prediction method combining the finite element method at low frequencies with ray acoustics at high frequencies is proposed. A complete methodological framework is established, including model construction, parameter optimisation and frequency-band connection, and is verified using a two-dimensional indoor case. The main conclusions are as follows.

(1) Compared with the finite element method, ray acoustics is less sensitive to mesh size, and its computational behaviour is governed mainly by the number of rays. Within a reasonable range, increasing the number of rays increases the computation time while improving prediction accuracy.

(2) The two-dimensional simulation results show that, in the 400-1000 Hz band, the spectral curves obtained by the ray acoustic and finite element methods have broadly consistent variation patterns. The errors at the centre frequencies of the one-third-octave-band sound pressure levels are all below 3 dB, and the mean absolute error is 1.14 dB.

(3) By coarsening the finite element mesh, the computation times of the finite element and ray acoustic methods are made comparable. Under the same

computational efficiency, the mean absolute error of the ray acoustic one-third-octave-band sound pressure level in the 400-1000 Hz band is 1.576 dB lower than that of the finite element method, demonstrating its advantage in this high-frequency range.

Acknowledgements

The authors gratefully acknowledge the support provided by the National Key R&D Program of China (2024YFF0508101)

References

[1] L.G. Kurzweil, "Ground-borne noise and vibration from underground rail systems", Journal of Sound and Vibration, 66(3), 363-370, 1979.

[2] J. Melke, "Noise and vibration from underground railway lines: Proposals for a prediction procedure", Journal of Sound and Vibration, 120, 391-406, 1988.

[3] C.E. Hanson, D.A. Towers, L.D. Meister, "Transit noise and vibration impact assessment", Federal Transit Administration, Washington, D.C., United States, 2006.

[4] Austrian Standards International, "Beurteilung der Einwirkung von Schwingungsimmissionen des landgebundenen Verkehrs auf den Menschen in Gebaeuden - Schwingungen und sekundaerer Luftschall: OeNORM S 9012", Austrian Standards International, Vienna, Austria, 2016.

[5] X. Li, Y. Chen, C. Zou, H. Wang, B. Zheng, J. Chen, "Building structure-borne noise measurements and estimation due to train operations in tunnel", Science of the Total Environment, 926, 172080, 2024.

[6] J. Sadeghi, M. Vasheghani, A. Khajehdezfuly, "Propagation of structure-borne noise in building adjacent to subway lines", Construction and Building Materials, 401, 132765, 2023.

[7] A.B. Nagy, P. Fiala, F. Marki, F. Augusztinovicz, G. Degrande, S. Jacobs, D. Brassenx, "Prediction of interior noise in buildings generated by underground rail traffic", Journal of Sound and Vibration, 293, 680-690, 2006.

[8] Q. Liu, D.J. Thompson, P. Xu, Q. Feng, X. Li, "Investigation of train-induced vibration and noise from a steel-concrete composite railway bridge using a hybrid finite element-statistical energy analysis method", Journal of Sound and Vibration, 471, 115197, 2020.

[9] B. Dawson, N. Mackenzie, Y.K. Lee, "Applications of statistical energy analysis to rail noise predictions", Proceedings of ACOUSTICS, 19(22), 2017.

[10] L. Savioja, U.P. Svensson, "Overview of geometrical room acoustic modeling techniques", Journal of the Acoustical Society of America, 138(2), 708-730, 2015,